Sweeping Jet Actuators - a New Design Tool for High Lift Generation

E. Graff[1], R. Seele[1] J. Lin[2],
& I. Wygnanski[3]

ABSTRACT

Active Flow Control (AFC) experiments performed at the Caltech Lucas Wind Tunnel on a generic airplane vertical tail model proved the effectiveness of sweeping jets in improving the control authority of a rudder. The results indicated that a momentum coefficient (C_μ) of approximately 2% increased the side force in excess of 50% at the maximum conventional rudder deflection angle in the absence of yaw. However, sparsely distributed actuators providing a collective $C_\mu \approx 0.1\%$ were able to increase the side force in excess of 20%. This result is achieved by reducing the spanwise flow along the swept back rudder and its success is attributed to the large sweep back angle of the vertical tail. This current effort was sponsored by the NASA Environmentally Responsible Aviation (ERA) project.

I. INTRODUCTION

Steady blowing was traditionally used to increase the lift of a wing by enabling larger flap deflections without causing the flow to separate. Although the use of blowing was driven mostly by the needs of naval aviation, the two popular mass-produced military airplanes relying on it were not intended for ship operation. They were the F-104 (some 2,600 airplanes were built) and the MiG 21 of which some 11,500 airplanes were produced. Blowing was used to slow down the landing speed of these airplanes and it did so on the F-104 by taking air from the last stage of the compressor and requiring momentum coefficients, C_μ, of approximately 8% for a reduction in landing speed of approximately 30 mph [1].

The lift increment attained by blowing is supposed to encompass two effects. Firstly, momentum is added to the boundary layer to overcome the frictional losses thus enabling the flow to proceed along the surface in spite of the adverse pressure gradient. Since the loss of momentum in the boundary layer is due to viscosity, keeping the flow attached became synonymous to overcoming the detrimental viscous effect, suggesting that the added momentum will improve the performance of the wing and bring it up to its ***inviscid limit***. Thus, when the flow is attached and the lift measured approximated the inviscid prediction, the momentum added to the flow by blowing suffices for separation control. In this case the lift increment $\Delta C_L \propto C_\mu$, and $C_\mu \leq C_{\mu r}$ is less or equal to some critical value $C_{\mu r}$. For larger input of momentum $C_\mu > C_{\mu r}$, the lift increment becomes smaller, $\Delta C_L \propto \sqrt{C_\mu}$ due to a "jet-flap" effect; a

[1] Contractor, California Institute of Technology, Graduate Aerospace Laboratories
[2] NASA Technical Lead, Environmentally Responsible Aviation Project
[3] Consultant, The University of Arizona, Aerospace and Mechanical Engineering Department

concept that is commonly referred to as "circulation control". The name "jet-flap" appeared because the thin jet departing the trailing edge (TE) of a wing at a large angle relative to the unperturbed free stream was initially modeled as flap extension [2]. The jet curves and approaches the free stream direction with increasing distance from the TE thus generating a pressure differential across the streamlines marking its borders, hence an increase in jet deflection increases the lift increment. The critical value of $C_{\mu r}$, dividing separation control from circulation control varies between $2\%<C_{\mu r}<5\%$. It depends on the specific application such as flap deflection, incidence, thickness of the wing, its shape, sweep and aspect ratio, as well as the extent of the deflected flap and its curvature. When blowing was applied from the shoulder of a highly deflected flap on a symmetrical airfoil whose length was less than 30% of the chord $C_{\mu r}$ became a function of flap deflection only and was approximately given by: $C_{\mu r}\approx 0.015\cdot\tan\delta_f$ provided the angle of incidence $\alpha=0^{\circ}$. Other reports indicate that circulation control requires a C_μ that is of the order of 10% although much larger and somewhat smaller values are quoted in the literature [3].

The concept of sequential separation control that is followed by circulation control was not seriously questioned to date, although there were indications that should have raised a red flag. Early experiments of blowing through variable slot widths indicated that narrower slots were generating higher lift than wider ones, suggesting that a given C_μ is more effective when it is accompanied by smaller quantity of fluid injected into the stream. Recent experiments [4, 5] of blowing and suction from the surface of a blunt elliptical airfoil concurred with that notion providing a new insight into the mechanics of separation control at low values of C_μ. In this experiment the slot width could be easily varied because the circular trailing and leading edges of the blunt airfoil were made of two parts that could rotate relative to each other thus changing the width of the slot.

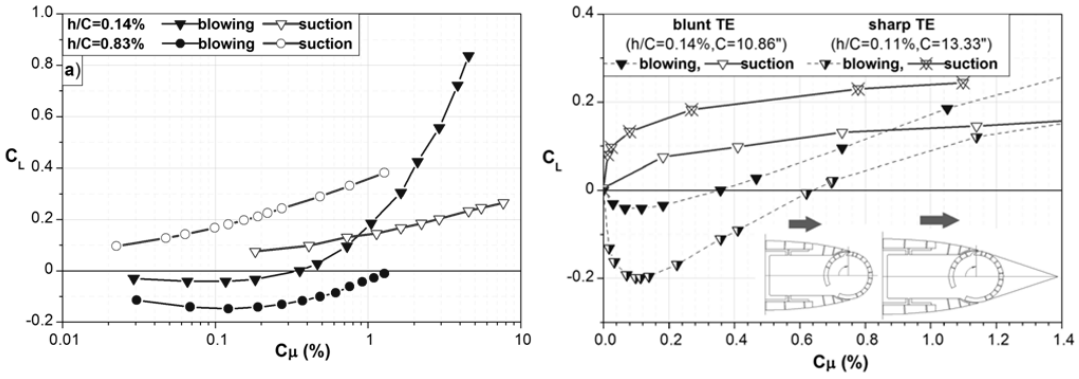

Figure 1 Blowing and suction near the trailing edge of an elliptical airfoil.

The blowing results shown in Figure 1, particularly those generated by a wide slot (h/C=0.83%) are deleterious generating negative lift for C_μ < 1%. Particle image velocimetry near the slot indicated that the low C_μ blowing displaced the streamlines farther away from the upper surface thus resulting in $\Delta C_L<0$. In these cases the jet velocities were comparable and not much higher than the free stream velocity, so the jet acted as a source located on the surface of the airfoil. Reversing the flow through the slot under otherwise identical conditions generated lift, because the suction through the slot brought those streamlines closer to the surface thus creating a potential flow sink on the upper surface. Adding a wedge to the trailing edge of this airfoil (inset in Figure 1b) accentuated the deleterious effects of blowing because the vertically displaced streamlines affected a larger surface. The sharp

trailing edge simplified the inviscid modeling of the flow by determining the location of the Kutta condition. The results shown in Figure 1b correspond to the narrow slot used in this experiment.

At higher C_μ blowing generates lift that surpasses the lift generated by suction. It usually occurs when the jet emanating from a two dimensional slot substantially exceeds the free stream velocity. Around that crossover threshold a narrow, high-speed jet flowing over the upper surface entrains ambient fluid that bends the streamlines toward the surface. In this case the jet momentum rather than its mass dominates the flow, enabling one to model its effect by a distributed sink (a line sink in two dimensional flow). The generation of lift by jet entrainment was demonstrated in 1964 [6] by examining the flow around a flat plate that was aligned with the stream and had a jet emanating tangentially to the surface. The streamline pattern obtained is reproduced in Figure 2.

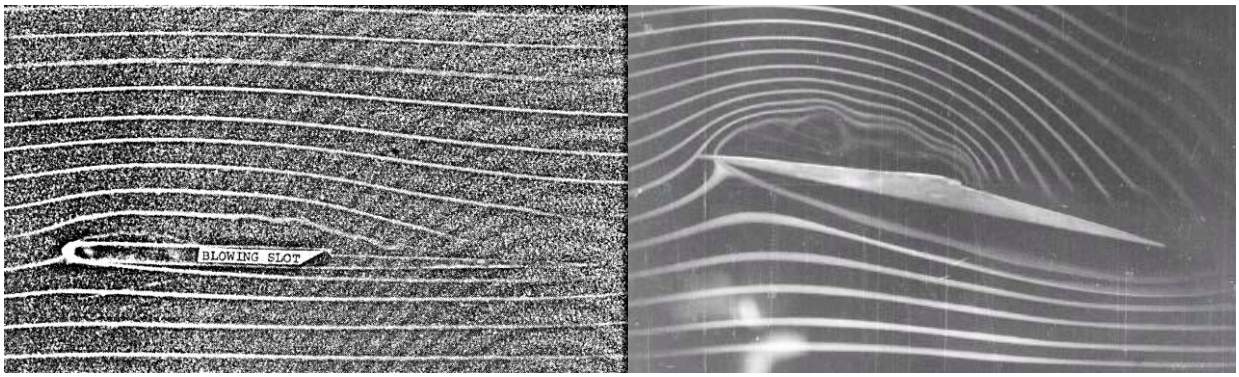

Figure 2 Streamlines on a flat plate and a triangular airfoil with a jet blowing over its upper surface.

Jet entrainment alters the pressure distribution on a surface of a body (a wing, an airfoil or a cylinder) thus enabling the flow to reattach to the surface even under the most adverse conditions shown in Figure 2b, where a sharp leading edge airfoil is at incidence relative to the oncoming stream [7]. The circulation around any airfoil that has a jet blowing over its upper surface is increased by the entrainment [6] and results in a lift increment that is proportional to $\sqrt{C_\mu}$. ***This model leads to the conclusion that there is no inviscid limit to the lift generated by a wing that uses blowing at low speeds, if ample momentum is available to provide the necessary entrainment.***

One may further ask whether it is possible to enhance the entrainment capability of a jet, and the sweeping jet actuation [8, 9] provides a plausible answer. One may also ask whether "jet entrainment" is a purely viscous phenomenon. Although this paper focuses on the practical question of lift enhancement we shall briefly discuss the mechanism of entrainment because it may lead to a more effective use of actuators.

When two parallel streams of greatly disparate velocities merge the discontinuity in their velocities, the interface is smoothed by viscosity. This creates a velocity profile that has an inflection point that is well represented by a hyperbolic tangent [i.e. $(u-U_1)/(U_2-U_1)=(1-\tanh y)$ where y is a distance measured across the flow from a location where the velocity is the arithmetic average of the two streams]. The most important characteristic of such velocity profile is the existence of the inflection point that makes it highly sensitive to an ***inviscid instability*** described by Kelvin and Helmholtz. This instability is so pervasive that the resulting mixing layer is turbulent in most aeronautical applications (even those associated with micro air vehicles). The state of the flow notwithstanding, the instability generates an array of large co-rotating eddies that grow in size by engulfing the fluid in their vicinity

(Figure 3). The engulfment process is (shown by arrows in Figure 3) may be enhanced and made more orderly by periodic excitation introduced at the origin of the flow. Very small amplitudes are needed to regulate and enhance the spatial growth of the instability and alter the entrainment capability of the mixing layer [10]. The frequency of the excitation determines the distance from the origin of the mixing layer to the location where the eddies are formed, their respective size and the strength of their entrainment capability.

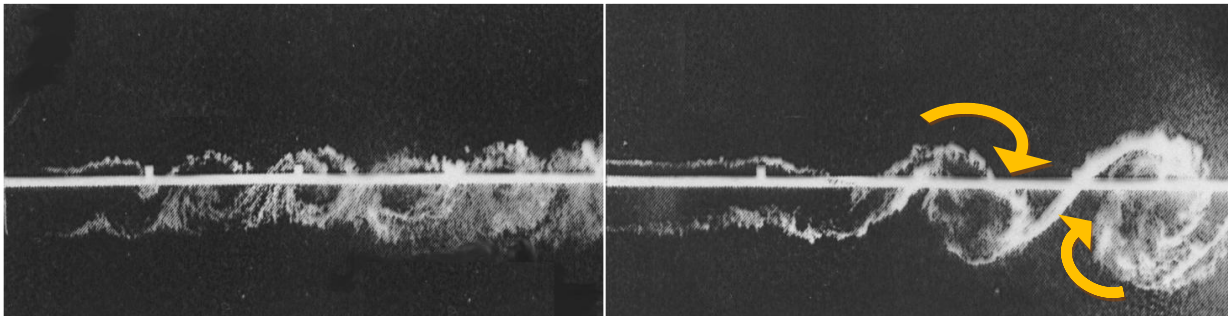

Figure 3 Large eddies in a turbulent mixing

Soon thereafter it was recognized that boundary layers on the verge of separation and shear layers that have already separated from a solid surface contain similar inflection points in their mean velocity profiles, and they too should be sensitive to the aforementioned instability. Thus, increasing the entrainment capability of these flows either lowers the pressure over the surface by bending the already separated mixing layer towards it, or it re-energizes the boundary layer that was about to separate and prevents separation altogether. Hence the concept of Zero Mass Flux (ZMF) separation control idea emerged [11].

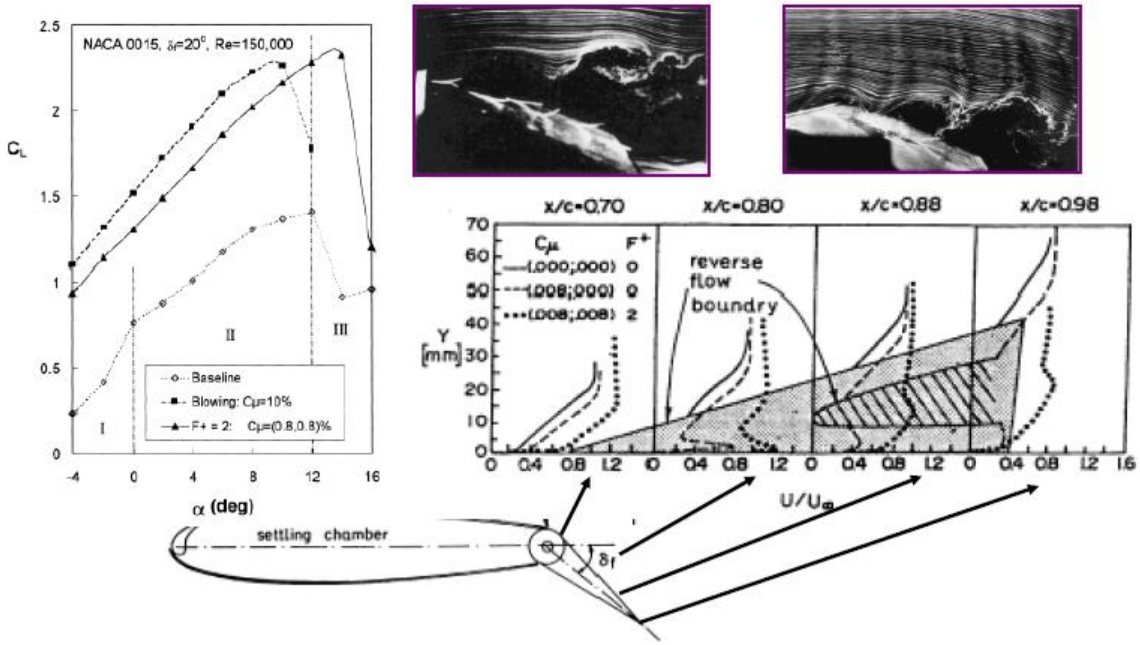

Figure 4 Control of separation on a flapped NACA0015 airfoil by ZMF [11].

Flow visualization by smoke (Figure 4) demonstrates the reattachment process over a deflected flap on an airfoil as a result of ZMF. Although the large eddies in the attached boundary layer are similar to those seen in the separated

flow, the mean velocity profiles measured over the flap are devoid of reversed flow. Experiments that compared the effectiveness of steady blowing to ZMF and oscillatory blowing showed that the oscillations substantially reduced the momentum required to attach the flow. In fact, the introduction of ZMF provided the same maximum lift as steady blowing while using only 20% of momentum input to achieve that task (Figure 4).

The role of the Kelvin-Helmholtz instability in separation control was most convincingly demonstrated on a generic flap [12, 13] where a small (2mm high) nozzle formed at the flap hinge allowed the introduction of periodic perturbations into the flow. Pressure taps on the flap were connected to dynamically responding sensors that were calibrated at the excitation frequency while transparent sidewalls maintained the flow two-dimensional and enabled a concomitant use of PIV (Figure 5b). The pressure traces shown in Figure 5a correspond to a flap deflection that exceeds the natural angle at which the flow reattached by $\Delta\alpha=6°$ thus at the initiation of actuation the flow was entirely separated. Phase-locked and ensemble averaged pressure coefficients $<C_p>$ were measured during the reattachment process since the activation of ZMF at a reduced excitation frequency of $F^+=f\cdot L_f/U=1.28$, where L_f represents the length of the flap. As could be expected, the phase-locked pressures over the entire surface of the flap are oscillatory, reflecting imprints of the passing structures generated by the excitation upstream. Close to the leading edge ($x/L_f < 50\%$), and throughout most of the reattachment process, each passage of a vortex is associated with an incremental decrease in the local mean pressure. The magnitude of the change is not constant along the flap as it depends on the excitation level and its frequency. The oscillations emanating at $x/L_f=0$ clearly amplify until $x/L_f\approx30\%$ and they decay farther downstream. Thus, the spatial growth of the instability plays an important role in promoting flow reattachment and the engulfment of fluid from the surface of the flap by the large eddies not only caused the reattachment but also maintained the attached flow thereafter.

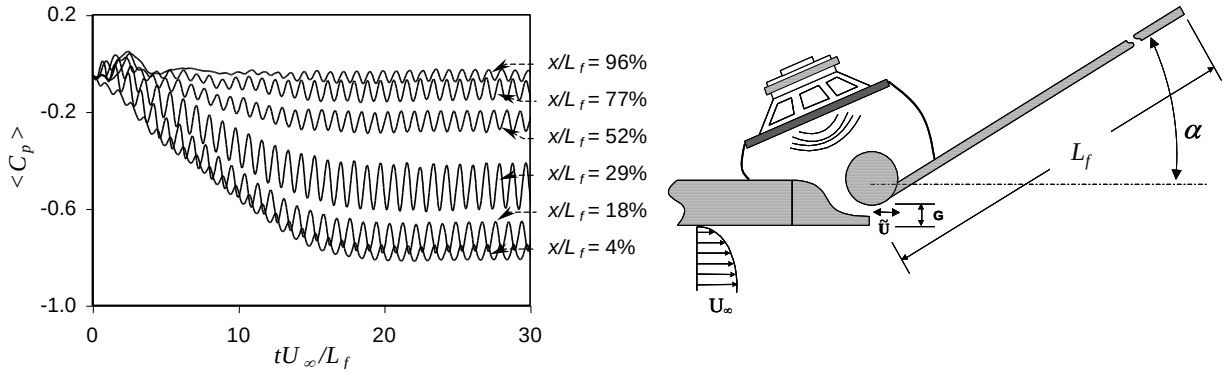

Figure 5 Temporal evolution of $<C_p>$ at various streamwise locations along the flap; Re_L =1.24×10^5, $\Delta\alpha_r$=6°, F^+=1.28, C_μ =0.05%.

The ZMF or synthetic jet idea was pursued at numerous laboratories [14-18] and its validity was demonstrated on two airborne vehicles: a "Pioneer" UAV in 1995 and on the XV-15 tilt rotor airplane in 2003 [19,20]. A blower and a rotary valve powered the AFC system in the Pioneer (Figure 6), oscillating a jet that emerged over a simple flap system. It increased the lift of the vehicle by 17% while requiring a C_μ<1%. The test on the XV-15 on the other hand was much more extensive. It used 52 electromagnetic actuators that provided the required ZMF actuation. The actuators were placed in individual bays near the leading edge of the flaps (Figure 6) and emitted their oscillations

through a segmented narrow slot. As a result the download created by the rotor wakes on the airplane in hover was reduced by enabling the flap to be deflected at an angle that exceeded the natural separation angle by 15°. Coincidentally the download allevaition was approximately 17% as it was in the Pioneer although the configuration and flight test conditions were differrent. The "Achilles Heel" of these tests were the actuators that were heavy and needed maintenance. Various other actuator types have been considered and tested since (e.g. plasma actuators, piezo-electric, mechanical, shape memory alloys, etc.) but none provided satisfactory results until sweeping jets were redsicovered.

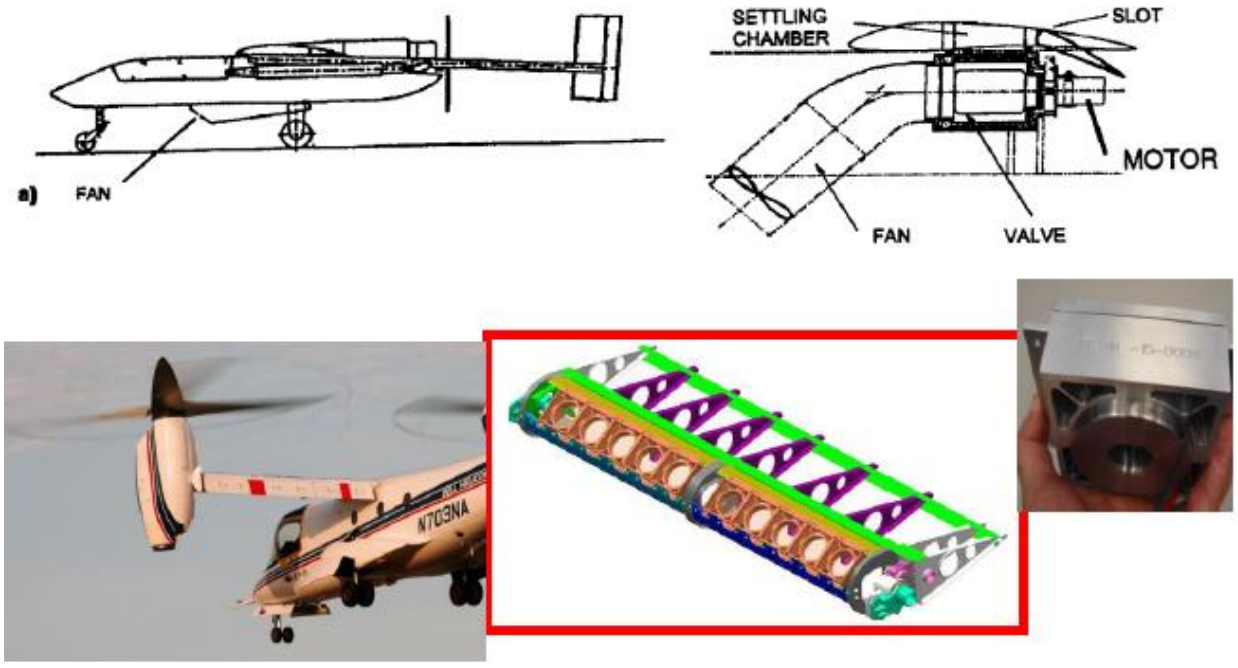

Figure 6 Airborne tests using active separation control.

The potential use of sweeping jet actuators (Figure 7) is attractive because they have no moving parts yet the jet that they emit sweeps back and forth from one side of the nozzle to the other, therefore interacting periodically with different regions of the boundary layer that is either separated or is about to separate. They seem to be able to entrain ambient fluid very effectively although the intricate details of this process is still unknown. The frequency of the sweeping motion and the jets residence time at each of the sweep extremities depend mainly on the shape and size of the actuator, among many other parameters that govern the character of the sweeping motion as well. Some actuator designs feature straight walls (Figure 7 right and center) but they proved to be slightly less effective than the curved wall actuator design shown schematically on the left. Other design variants have a triangular diverter at the exit making the jet bi-stable which allows it to oscillate between two predetermined positions. The flow inside an actuator and actuator development was and still is actively investigated at a number of laboratories [9, 21, 22] and in some instances it is backed by CFD [23].

Figure 7 Typical sweeping jet actuators and the interior flow in them [23].

The air passing through the "Power Nozzle" (marked on the left of the left most schematic in Figure 7) attaches itself to one of the solid surfaces forming the walls of the main cavity of the actuator (in the present case it is shown to be attached to the upper surface). The jet curves as it rushes to the outlet which concomitantly increases the pressure at the inlet to the upper feedback channel. This creates flow in the feedback channel that pushes the entering jet to the opposite surface and repeats the process. The oscillation can therefore be considered two dimensional in nature although the jet itself is three dimensional and can be inclined to the downstream surface of the wing at any angle. Its frequency is determined by the dimensions of the feedback channel and its spanwise deflection angle depends on the detailed design of the actuator. The jet in the rectangular, straight wall actuator also curves enclosing a bubble near the surface to which it attaches itself (Figure 7 right) and it partially impinges on the interior walls of the exit nozzle increasing the pressure at the inlet to the feedback channel.

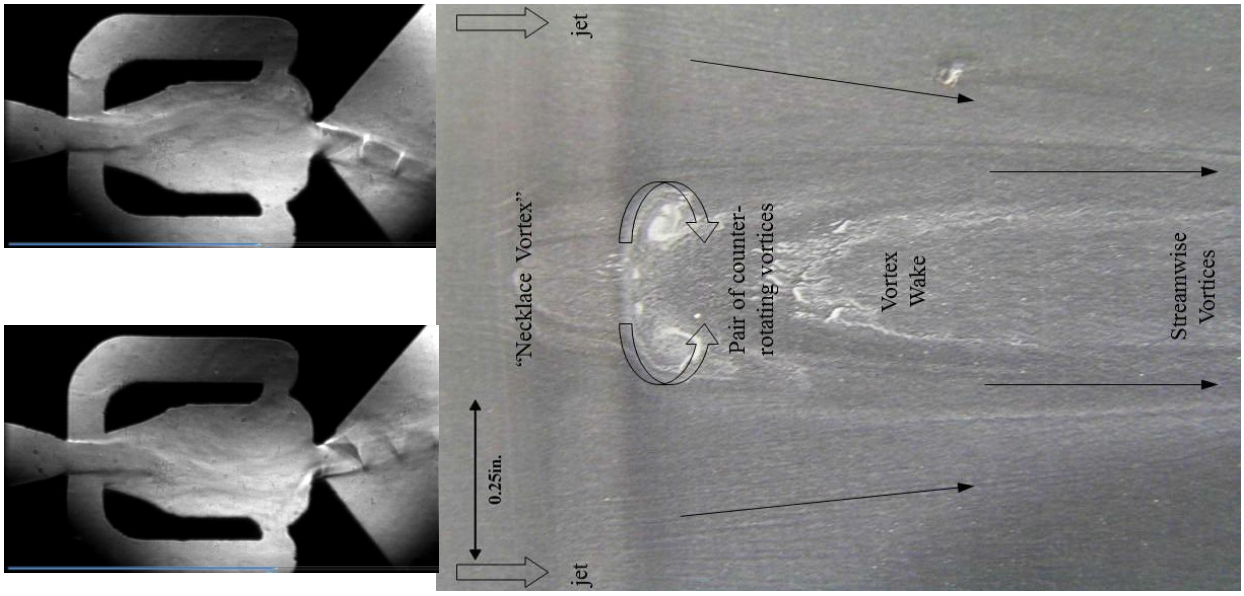

Figure 8 Compressible flow through the actuators [21] and an interaction between two sweeping jets and separated flow over a flap [9].

The sweeping jet actuators were originally developed during the nineteen fifties at the Harry Diamond Research Laboratories to be used in analog computers and fluidic amplifiers. Currently, they are used in cars for windshield washers systems, shower heads and irrigation systems. Since their commercial applications involve water the effects of compressibility where never seriously addressed. Since these devices have only recently been used to control

separation for aeronautical applications, the presence of shock waves and nozzle choking was found to have significant importance (Figure 8) [22]. A completely different yet important field of endeavor concerns the interaction between the sweeping jets and the external flow in the boundary layer.

An exemplary surface flow visualization pattern over a deflected flap is shown in Figure 8. In this case the flow reattached due to the presence of the sweeping jets that are located just beyond the left boundary of the picture with their spanwise location being marked by the open arrows. Directly downstream of the actuator nozzles a rapid jet is flowing near the surface. Centered between the jets, a wake is formed in the interaction region. The sweeping plane of the jets is inclined to the downstream surface by approximately 30°. Thus when the two adjacent jets interact (or perhaps even collide) they form a fountain whose axis is fairly normal to the surface. The fountain flow then bends in the direction of streaming which in turn creates a kidney shaped jet that possesses two counter rotating streamwise vortices. However, at the base of the fountain the oncoming ambient flow may be brought to stagnation which results in the formation of a necklace vortex that wraps itself around the fountain. The vorticity in the separated flow upstream changes its orientation from spanwise to streamwise direction reinforcing the pair of counter rotating streamwise vortices of the fountain. This brings high speed fluid toward the surface in the wake of the fountain. Consequently sweeping jets act similar to vortex generators that sweep along the span in addition to providing momentum in the direction of streaming. The mushroom shape seen in Figure 8 represents the footprint of the fountain flow, while the "U" formed upstream of it corresponds to the necklace vortex. The distance between these two patterns increases with increasing C_μ.

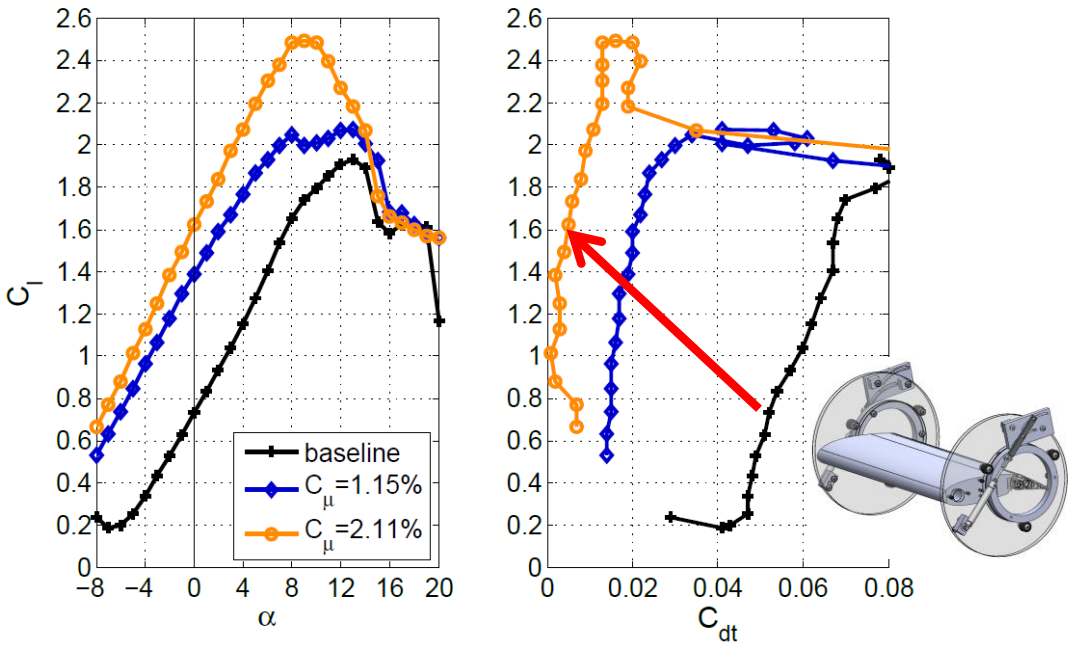

Figure 9 Lift and drag characteristics at various levels of C_μ, δ=20°, Re=4*10^5 [24].

Sweeping jets provide an effective tool for delaying separation even at low levels of momentum input, in spite of the fact that their detailed interaction with the boundary layer is still unknown. Take the NACA0021 flapped airfoil as an example (Figure 9). For a flap deflection δ = 20° and in the absence of actuation the flow over the flap is

separated for the entire range of applicable angles of attack, α. A C_μ input of 1.15% sufficed to attach the flow over the flap for small α, thereby increasing the lift by almost a factor of 2 and decreasing the drag at least by a factor of 3. Augmenting the momentum input further does not improve the lift significantly after the flow over the flap had already attached, but a reduction in drag is evident due to the additional thrust input of the jet. Thus at C_μ = 2.11% and α=0° C_L increases from 0.73 to 1.6 (red arrow on Figure 9) but *L/D* increases from approximately 15 to 60 even after accounting for the C_μ input as thrust. Thinner airfoils and smaller chord flaps generally show less improvement in lift generation by these jets but the overall results remain impressive.

The results of Figure 9 provided the impetus to put AFC into practice and the most obvious and least risky application is the vertical tail of a twin engine airplane whose size is determined by the eventuality of losing an engine during takeoff and low speed climb. The vertical tail represents a large surface that is hardly used under normal flight conditions although it is indispensable during the aforementioned "engine out" emergency and it is also needed during cross-wind takeoff and landing. The safe landing of the tailless B-52 shown below attests to some of its redundancy in non-critical situations. Although seldom used to its full capability, the vertical tails presence adds drag and weight to the aircraft for the entire flight envelope thus increasing fuel consumption. Active Flow Control (AFC) devices that delay flow separation over a highly deflected rudder may enable a smaller vertical tail to provide the control authority needed during emergency, but the broad purpose of AFC is to extend and augment the capabilities of lift generation by flaps and control surfaces beyond the natural separation of the flow. AFC may become a tool that interacts with all the other variables affecting the shape of the vertical tail, and the level of that interaction is still to be determined. The present experiment was initiated to establish the efficacy of a system that uses sweeping jet actuators at the rudder hinge. It breaks new ground in AFC applications because of the large sweep back of the vertical tail – typical sweep back of the tail surfaces exceed the sweep back of the wing by 10-15° – and its relatively low aspect ratio. The present experiments were carried out on a vertical tail model at low speed (U<100 knots) at mean chord Reynolds Numbers just below $1.5*10^6$.

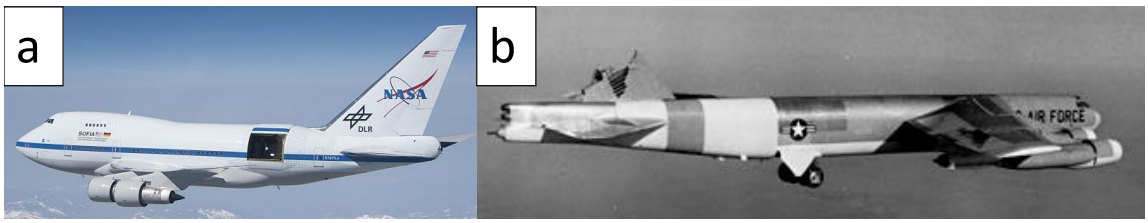

Figure 10 (a) short body version of a 747, credit: NASA/ Jim Ross; (b) A B-52H that lost its vertical tail in clear air turbulence, credit: Wikipedia/ United States Air Force.

II. Experimental Setup and Instrumentation

The base vertical stabilizer model has a NACA 0012 shape and was designed based on publicly available information and tested at the California Institute of Technology's Lucas Wind Tunnel. The wing is tapered and swept back by Λ=42° at the leading edge (LE), has a 35% flap, a 0.54m MAC, a span of S=1.09m and features a fairing similar to what is used on a real stabilizer to smoothen the transition between fuselage and stabilizer. The closed loop wind tunnel's test section is 6ft (1.8m) high and 5ft (1.5m) wide and is operated at speeds of up to 50m/s

for this experiment. A ground plane that houses a six component strain gage balance was used to support the model. This ground plane decreased the effective height of the wind tunnel to 1.3m. A windshield was installed around the base of the model and attached to the ground plane to shield around the mounting hardware and minimize the effect of the developing boundary layer at the wall. To minimize Reynolds number and transition related effects, tripping dots were applied at *x/c*=5% on the models suction side and at *x/c*=10% on the pressure side.

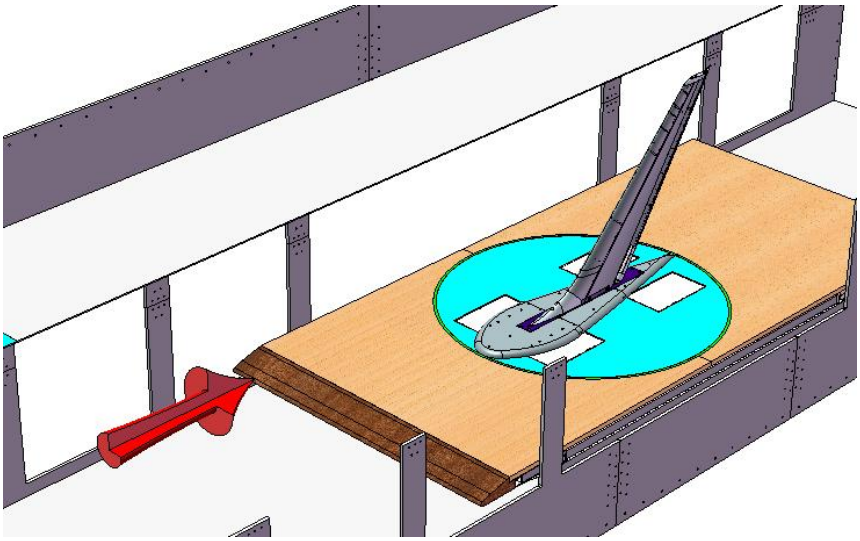

Figure 11 Vertical Stabilizer Setup in the Lucas Wind Tunnel test section.

Pressure distributions at various spanwise and chordwise locations were evaluated with a Pressure Systems, Inc. 8400 system. The stabilizer is equipped with roughly 230 static pressure ports arranged in a spanwise and chordwise grid oriented relative to the LE of the main element and the rudder. The three major chordwise rows (Figure 12) feature between 36 and 39 static pressure ports and are located at *z/b*=43%, 71% and 90% relative to their starting point at the LE of the model. A number of additional ports are used to assess the flow in spanwise direction.

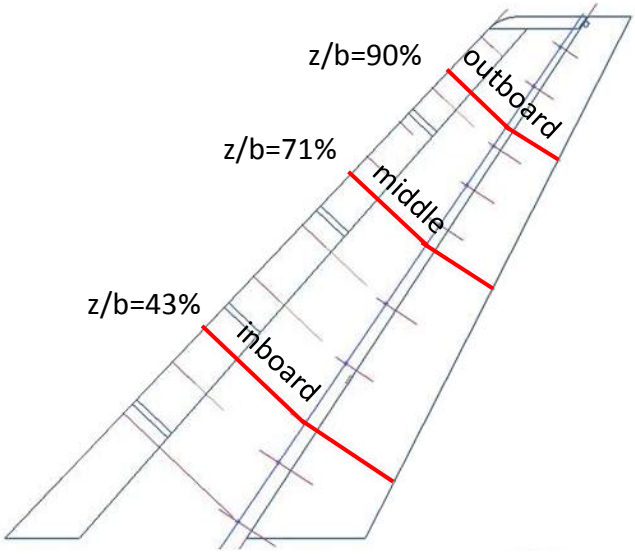

Figure 12 Position of Chordwise Pressure Tap Rows (shown without fairing).

The sweeping jet actuators were supplied with compressed air through the root of the model. Hose forces were assessed in various different arrangements and found to be negligible. The air supply was controlled by an electronic pressure regulator while the ejected mass flow was recorded by a flow meter which was digitally corrected for pressure and temperature. A maximum of 32 actuators were located at the trailing edge of the main element. The ejection angle relative to the surface is 10° and the narrowest achievable spacing is 3% of the span. Individual actuators can be blocked with plugs thereby achieving different spatial distributions.

III. Results

All results have been normalized such that the coefficients at 0° sideslip and 60% rudder correspond numerically to 1. Actuator spacing has been normalized by the span and actuator size by the area of the largest nozzle. The rudder deflection angle has been normalized by an arbitrary maximum angle.

A. Evaluation of rudder performance that is aided by AFC

Most of the experiments were carried out on the AA model that is considered to be a typical modern vertical tail used by industry. The lift (side force) and drag experienced by this model at various rudder deflection angles, δ_R, and side slip angles, β, are shown in Figure R 1. These were obtained at free stream velocities of 40 m/sec corresponding to Reynolds numbers of 1.35M. The results were independent of Reynolds number with the exception of the lowest measured case (20 m/sec), nevertheless trip dots were placed at x/c=0.05 on the suction side and they increased the side force generated by the vertical tail by ever so slightly.

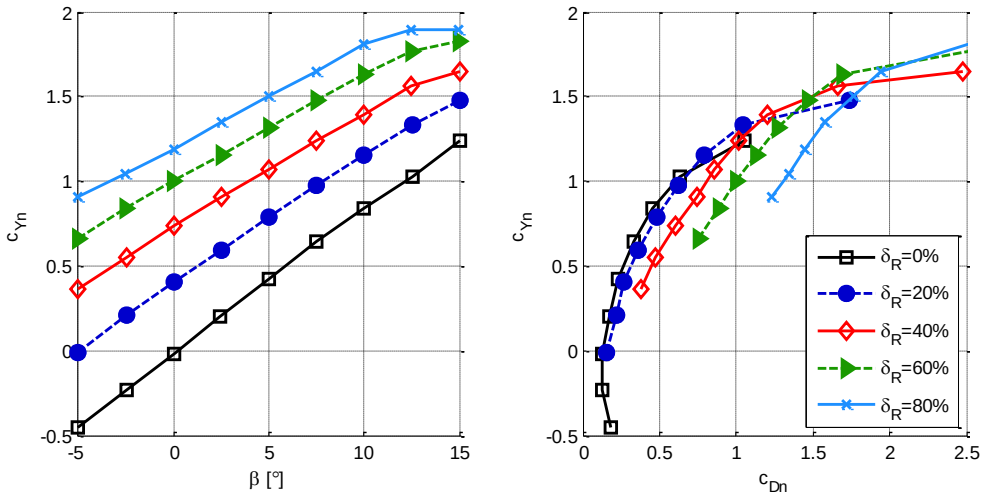

Figure R 1 The side force and drag polar of the AA model as a function of rudder deflection.

Increasing the side slip angle resulted in a linear increase in side force, C_{YN}, provided β<10°. At β>10° the vertical tail stalls at δ_R=80%, while at smaller values of δ_R>0% partial separation of the flow is responsible for the observed reduction in C_{YN} increment with increasing β>10°. In fact the slope of C_{YN} vs. β lines decreases from $(dC_{YN}/d\beta)_{normalized}$=0.082 corresponding to δ_R=0% to 0.062 at δ_R>80% suggesting a thickening of the boundary layer and some regional separation occurring at large rudder deflections. This also reflects on the increase in drag measured at a given C_{YN} with increasing δ_R. There is no obvious drag penalty corresponding to δ_R<20% but for

δ_R=40% the drag is substantially higher even at negative β. A considerable amount of the increase in drag is due to lift (i.e. induced drag). Since prolonged side-slip is not an option en route or whenever a contact with a runway is concerned (with the exception of the B-52) it is the yaw authority that matters.

The side force generated by a conventional rudder at small deflection angles (prior to the occurrence of separation) is linearly proportional to δ_R. An increase of rudder deflection beyond the δ_R corresponding to the initiation of separation reduces rudder effectiveness by reducing $dC_{Yn}/d\delta_R$ (Figure R 2) while concomitantly increasing drag. For the AA configuration the initial signs of reduced effectiveness occur at $\delta_R \approx 20\%$ and it becomes more pronounced for $\delta_R > 60\%$ which most likely determines the maximum effective rudder deflection for similar configurations. Thus the need for a prescribed side force at different stages of the flight envelope determines the size of the rudder and the vertical tail. Sweeping jet actuation at C_μ=0.5% maintains a constant ($dC_{Yn}/d\delta_R$) up to $\delta_R \approx 50\%$ while it requires a C_μ=1.5% to increase the linear dependence of C_{Yn} up to δ_R=60%. At that point the side force coefficient has increased to 1.5 thus exceeding the side force generated by the vertical tail by 50%.

The jet momentum coefficient, C_μ, was used as the leading parameter affecting the state of the flow over the rudder because it is traditionally used whenever blowing is applied to control flow separation and circulation over wings. The length scales or area ratios used in the definition of C_μ may be unique for flapless airfoils but their uniqueness is lost when flaps and slats are introduced to airfoils and even more so for finite wings. In the case of a highly deflected rudder it may be the rudder area that determines the momentum required to control the flow and not the area of the entire vertical tail. The use of sweeping jets emanating from discrete sources provides additional length scales of significance e.g.: the size of the actuators' nozzles, their aspect ratio as well as the distance between adjacent actuators. These and other parameters have to be carefully considered when contemplating application to an airplane.

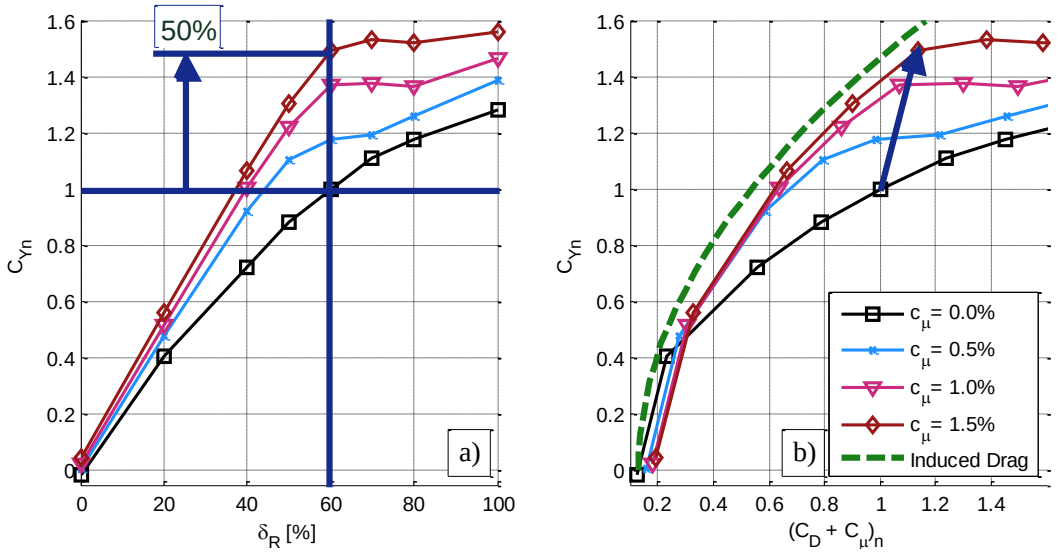

Figure R 2 Lift and Drag polars for β=0° at U_∞=40m/s with 3% spacing.

The increase in drag resulting from the use of sweeping jets at various rudder deflections is shown in Figure R 2b. The drag polars plotted in this figure presume that the entire jet momentum is recovered as thrust, thus the abscissa

represents $(C_D + C_\mu)_n$ instead of the traditional C_D. The arrow originating at (1; 1) in this figure and pointing at (1.1; 1.5) represents the increase in $(C_D + C_\mu)_n$ due to 50% increase in side force by application of Active Flow Control at δ_R=60%. This increase is attributed to the induced drag because of the increase in side force (lift). The dashed green line shown in Figure R 2b represents the increase in drag due to lift by assuming an elliptical load distribution on a wing having an aspect ratio corresponding to twice the height of the vertical tail. The factor of two arises from the image representing the floor of the tunnel. It clearly predicts the increase in induced drag encountered, although the lift distribution on the vertical tail is not elliptical.

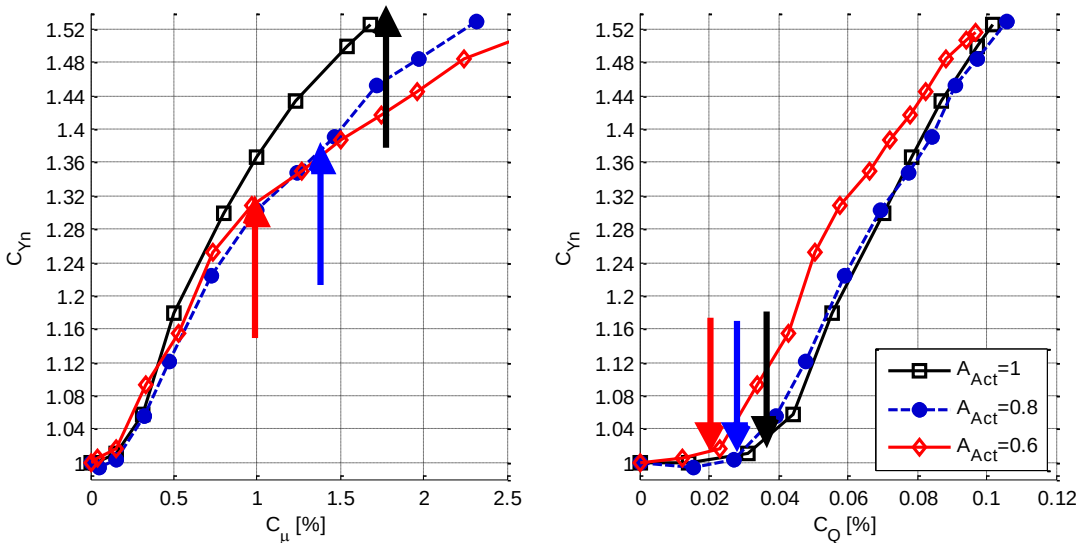

Figure R 3 Different actuator sizes, lift vs. momentum and mass flow for δ_R=60%, β=0° at U_∞=40m/s with 3% spacing (arrows pointing up indicate U_j=U_c; arrows pointing down indicate U_j=3·U_∞)

One may fix the rudder deflection angle (δ_R=60%) and observe the effect of increasing C_μ on the increase in C_{Yn} for three different sweeping jet nozzle areas that decreased from 1 to 0.8 to 0.6 (Figure R 3). It appears that as long as C_μ is small (C_μ<0.5% in this case) and the flow though the nozzles is subsonic, the C_{Yn} generated by AFC is not sensitive to the nozzle size or its throat aspect ratio. However, once the flow through the nozzle throat becomes supersonic (dC_{Yn}/dC_μ) decreases due to the inhibited sweep angle of the sweeping jet. In Figure R 3a, the arrows pointing up indicate where U_j equals the speed of sound U_c. One may suggest that compressibility affects the control authority of the sweeping jets although the true effects are unknown. It is recognized that a steady supersonic jet has a lower spreading rate than a subsonic one (i.e. it is less effective at entraining ambient fluid than a subsonic jet of the same jet momentum) and the same may hold true for the sweeping jets, particularly if compressibility affects the frequency of the sweeping motion. The dependence of the side force on C_Q is shown in Figure R 3b. It further indicates that a threshold value of ($U_j \approx 3 \cdot U_\infty$) is required before any benefits can be reaped from the sweeping jets for this specific rudder deflection. As long as U_j is of the same order of magnitude as U_∞ and the flow is incompressible the volume flow emanating from a nozzle simply displaces the streamlines outward. Once $U_j >> 3 \bullet U_\infty$ and the jet attaches to the surface (wall jet), entrainment of ambient fluid bends the streamlines toward the surface which enables the flow to turn around the deflected rudder and avoid separation. The threshold C_Q is smallest for the

smallest nozzle because (U_j/U_∞) is the largest for a given jet volume flow. (In terms of its effect on the outer potential flow, a slow jet may be represented by a point source while a fast one has to be modeled as a line sink whose local strength is diminishing along the path of the jet.) Earlier studies have shown [4] that the most effective separation control by steady blowing occurs when the jet emanates from the narrowest slot placed near the natural separation location.

The mass flow supplied to the vertical tail and the pressure in the settling chamber leading to the sweeping jet actuators, can easily be measured. On the other hand, measuring the average jet velocity emanating from the actuators' nozzles requires extensive effort, or it can be calculated using crude one dimensional approximation. Thus instead of analyzing the data in terms of momentum one may define a figure of merit that is based on the easily and unambiguously measured parameters. A power coefficient, C_π, that is dependent on the pressure difference between the settling chamber upstream of the actuators and the free stream, p_{ch}, and the total volume flow Q:

$$C_{\Pi} = \frac{Q \cdot p_{ch}}{0.5 \cdot A_{ref} \cdot \rho_\infty \cdot u_\infty^3}$$

Since the volume flow multiplied with chamber pressure has the dimension of power it would allow one to judge the efficiency of the actuation system by taking the ratio between C_π and the power required by the system to generate the flow.

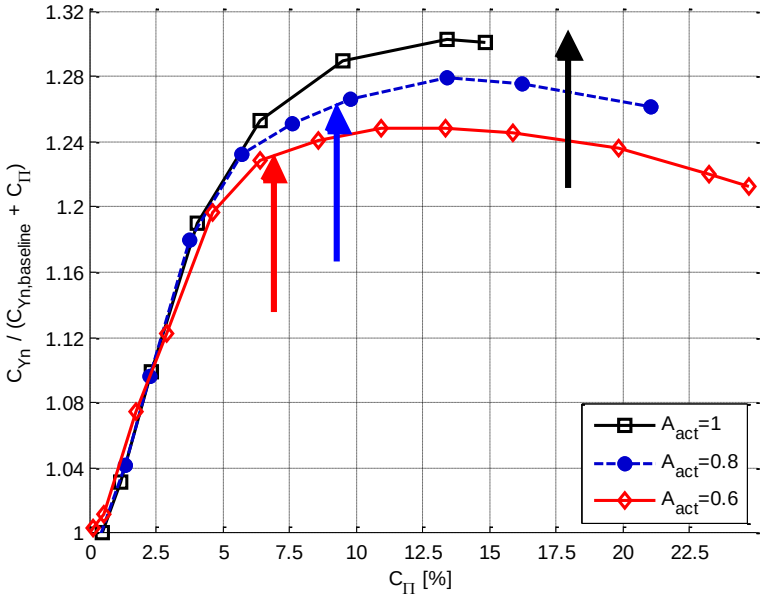

Figure R 4 Figure of merit, FM, provided by different actuator sizes, δ_R=60%, β=0° at U_∞=40m/s with Sp=3% (arrows pointing up indicate $U_j=U_c$)

On the other hand, a ratio $C_{Yn}/(C_{Yn,baseline}+C_\pi)$ establishes a simple figure of merit that is indicative of the value of the sweeping jets to the enhancement of the control authority of the rudder (Fig. R4). While the results shown in Figure R 3b suggest that using smaller orifices consumes less mass flow to provide a given increase in C_{Yn}, Figure R4 indicates that it does so at a cost of higher power required provided C_π,<13 because all the three sizes of actuators

tested attain the highest figure of merit at this level of C_{π}. The additional C_{π} required to achieve a targeted C_y is associated with higher p_{ch} used by smaller actuators. Both C_{π} and C_{μ} lead to similar conclusions suggesting that the largest actuators perform more efficiently than the smaller ones ostensibly because they choke at higher respective levels of each parameter. However, when considering the application problem in its entirety, smaller mass flow and smaller diameter ducts may become decisive factors.

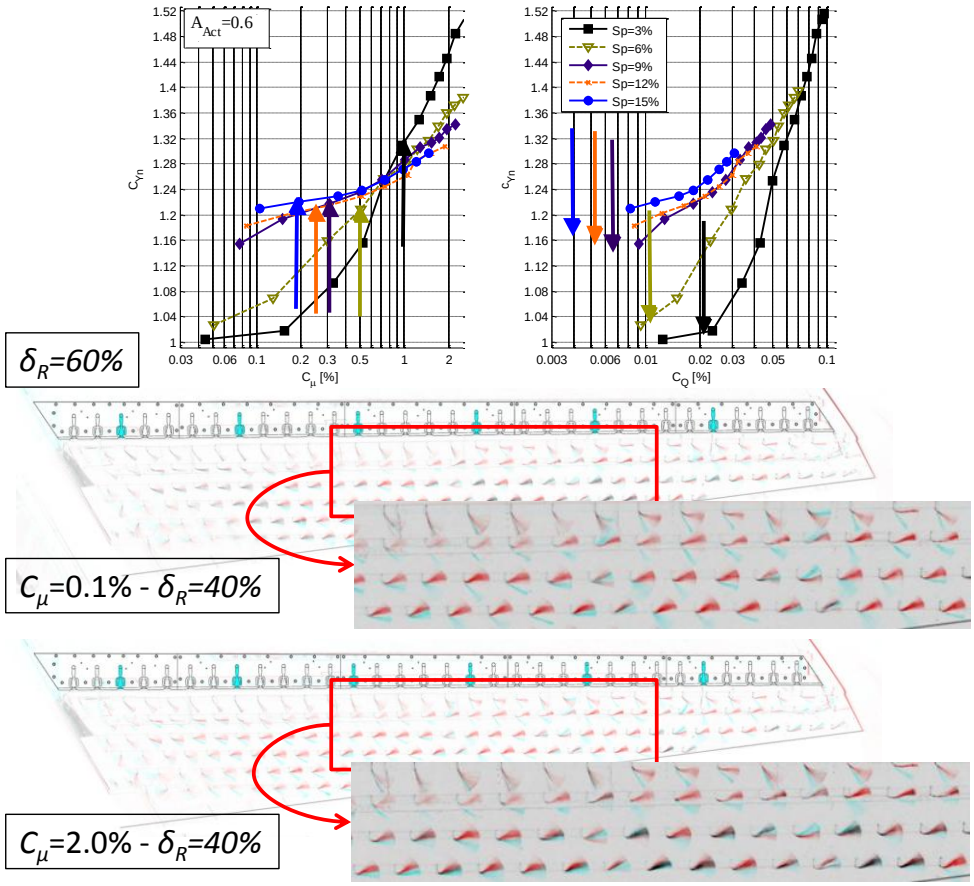

Figure R 5 Efficiency of different actuator spacings at δ_R=60%, β=0° and U_∞=40m/s with actuators; A_{act} = 0.6 (arrows pointing up indicate $U_j=U_c$; arrows pointing down indicate $U_j=3\cdot U_\infty$); the pictures show the alteration of flow direction by AFC. Top C_μ=0.1% & δ_R=40% Bottom C_μ=2.0% & δ_R=40%.

One may maintain a constant average momentum input for a given chamber pressure by either changing the actuator size or changing the distance between adjacent actuators. Figure R 5 shows the effects of spacing, Sp, on actuators with an orifice size of 0.6 at a prescribed δ_R=60%. For a given C_μ<0.8% increasing the distance between adjacent actuators increases the C_{Yn} generated by the vertical tail. At very low C_μ an increase in spacing implies a substantial increase in U_j that lowers the threshold level at which the jet starts entraining ambient fluid but it also provides a jet curtain that stops locally the spanwise flow along the rudder. This is not apparent from the integral values that consider the entire surface of a wing or the rudder. The reorientation of the flow in the direction of streaming (green tufts in Figure R 5c) and the corresponding effect it has on the production of side force by the vertical tail might be specific to the interaction between backward sweep of a wing and high speed actuation. This could not have been

observed on a straight wing or on a tapered one and in this case the sweeping motion of the jets may even be detrimental to the reorientation process. By quintupling the distance between actuators to 15% one may generate a 20% improvement in C_{Yn} at C_Q=0.01% or C_μ=0.1%. Tufts indicate that the flow changes direction at the lowest C_μ measurable. At high C_μ the individual jets reach the trailing edge of the rudder creating cells of partly recirculating chordwise flow. However, at high C_μ the actuators may have already redirected the local spanwise flow. The sparsely spaced nozzles choke early and shocks may appear at their exit partially accounting for the rapid decrease of the slope (dC_{Yn}/dC_μ). When the jets are supersonic large areas between the actuators remain unexposed to the positive effects of actuation.

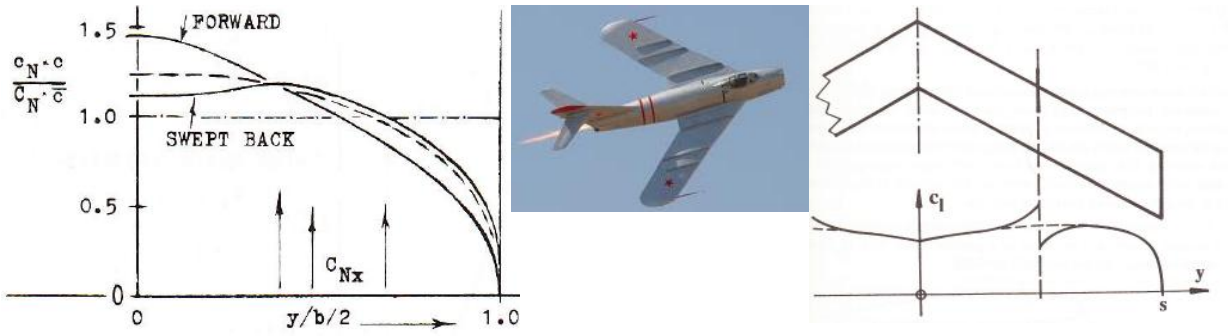

Figure R 6 The role of a fence on a swept back wing.

It is well known that the spanwise load distribution on a swept back wing is far from being elliptical. In fact the load at the root of the wing has a local minimum and increases in the spanwise direction before decreasing rapidly toward the tip (see Figure R 6 representing three sweeps -45°; 0° & 45° having an aspect ratio of 4 and a relatively small taper ratio). For the case shown in Figure R 6, the maximum load occurs at approximately ½ of the span and they are representative of the vertical tail situation that is also swept back at approximately 45°. This type of a wing stalls first at its tip and the separated region propagates inboard. A fence that spans the chord and is wrapped around the leading edge reduces the load on the outboard portion of the wing (Figure R 6) by somewhat delaying the flow separation. The influence of the fence is very local and it was mostly used to improve the maneuverability of military aircraft. By requiring that the fence will be a streamline the flow near the fence is parallel to the free stream and losses associated with the spanwise flow near the tip are reduced and ultimately resulted in abrupt "nose up" pitching moment near C_{Lmax}. Consequently, fences provided some advantages at high incidence but increased the drag during cruise. Sparse weak blowing near the rudder hinge substantially reduced the spanwise flow, particularly for the outboard 60% of the rudder. This change of flow direction has a global effect on the side force (lift) increasing it by more than 20% even for minimal momentum inputs.

Observations carried out on a flapped λ-wing suggested that fully attached flow over such wing had a strong spanwise component near the trailing edge of the slightly deflected flap (δ_R=10°). The flow is attached because the tufts are completely stationary (steady) and the photographs shown in Figure R 7 represent an average of 250 individual pictures that were superposed on top of each other. One tuft located near the juncture of the λ that was also a flap juncture oscillated and it shows as a fan in the picture (see red circle). Sweeping jet actuation near the flap hinge changed the direction of the flow over the flap and increased the lift by approximately 30%. It appears

therefore that the actuators on a swept back wing have two very different but perhaps equally important functions: (i) to reduce the spanwise flow component (ii) retain attached flow over a surface at incidence or flap deflection that exceeds the natural separation angle. The first task applies only to swept back lifting wings while the second is much more general.

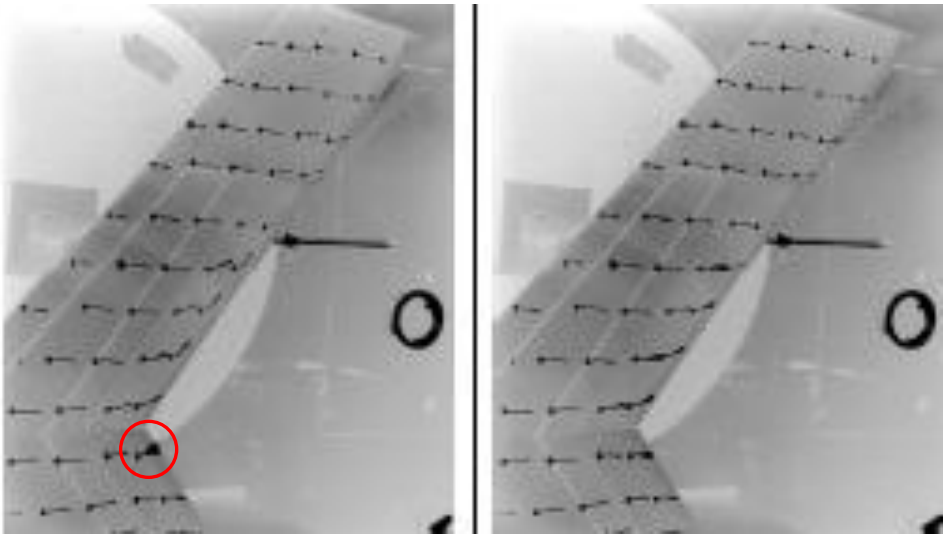

Figure R 7 Attached flow on a λ wing δ=10° and α=4°.

Generally, to achieve a desired improvement in C_{Yn}, there is a confluence of geometrical parameters such as rudder chord, its deflection and its sweepback angle as well as other AFC related parameters (i.e. C_{μ}, actuator spacing and actuator size) that are closely coupled and their respective effect on the flow might be partly interchangeable. Although there are many possibilities for optimization there is a hierarchy of choices to be made depending on the models geometry and the available input for the actuation.

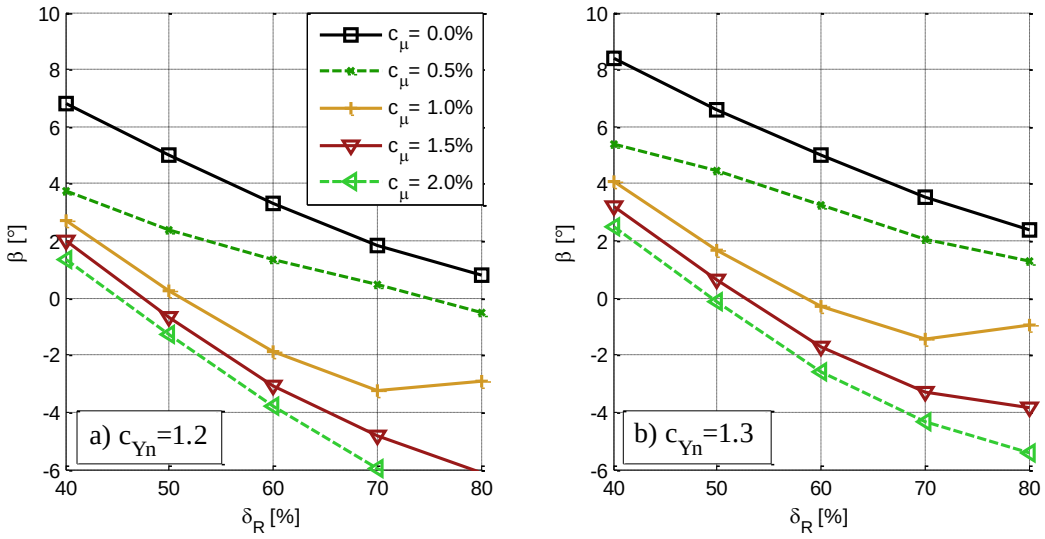

Figure R 8 Necessary rudder, C_μ side slip combination achieving a predefined C_{Yn}=1.2 and 1.3, on installed 0.8 area actuators spaced at spacing of 3%.

When sizing a vertical tail or generally a wing one may use figures akin to Figure R 8 where it is shown how a given C_{Yn} can be provided by a combination of δ_R, β, or C_μ on a finished product in which all other engineering parameters were already predetermined. Suppose the conventional rudder (C_μ=0) would not be able to provide the needed side force of C_{Yn}=1.2 at β=0° even at δ_R =80% (Figure R 8a). As a result the vertical tail has to be larger in order to provide the necessary yaw authority. Using sweeping jet actuation, a C_μ=1% would fulfill such a requirement at δ_R=50% while avoiding side slip. This can enable a reduction in size of the rudder. In case C_{Yn}=1.3 is required a Cμ=2% would be needed to avoid side slip or the rudder deflection would have to be increased to δ_R=60% if C_μ of 1% could not be exceeded (Figure R 8b). This example suggests how AFC can enable a reduction in the total size of a vertical tail because the desired normal force generated can be achieved by rudder deflection, but also by AFC. For the specific case of a vertical stabilizer the goal is to reduce the overall size without losing the ability to control the airplane in critical situations. The results plotted in Figure R 8 show that the necessary yaw could be provided by a smaller size tail.

Thus far the actuators were uniformly distributed along the span and their input was uniform as well. The value of this uniformity should now be questioned. The results plotted in Figure R 9a show the effect of methodical removal of actuators from the tip region. The ordinate represents the difference between the measured C_{Yn} while some actuators were inactive and all the actuators being used at a given C_μ, while the abscissa represents the inactive tip length in percentage of span. It transpired that stopping the actuation at 85% of the span has no deleterious effect on C_{Yn} up to the highest C_μ tested in this experiment.

Removal of actuators from the root region had an immediate effect on the C_{Yn} generated by the rudder at the highest C_μ=1.7% that was used for this configuration (Figure R 9b). If however, C_μ=1% is not exceeded at this δ_R, one could only focus the actuation on the central 60% (by stopping short of 30% from the tip and approximately 10% from the root) of the span without noticing degradation in performance. In fact for low $C_\mu \approx 0.5\%$, one would be more

effective actuating in the central region of the vertical tail. The optimization of the extent at which sweeping jet actuators are effective depends on the rudder deflection, thus one should place limits on the combined effect of rudder deflection, C_μ and on the spanwise extent at which AFC is carried out. This observation led to an investigation of regional application of AFC that was in part triggered by CFD input.

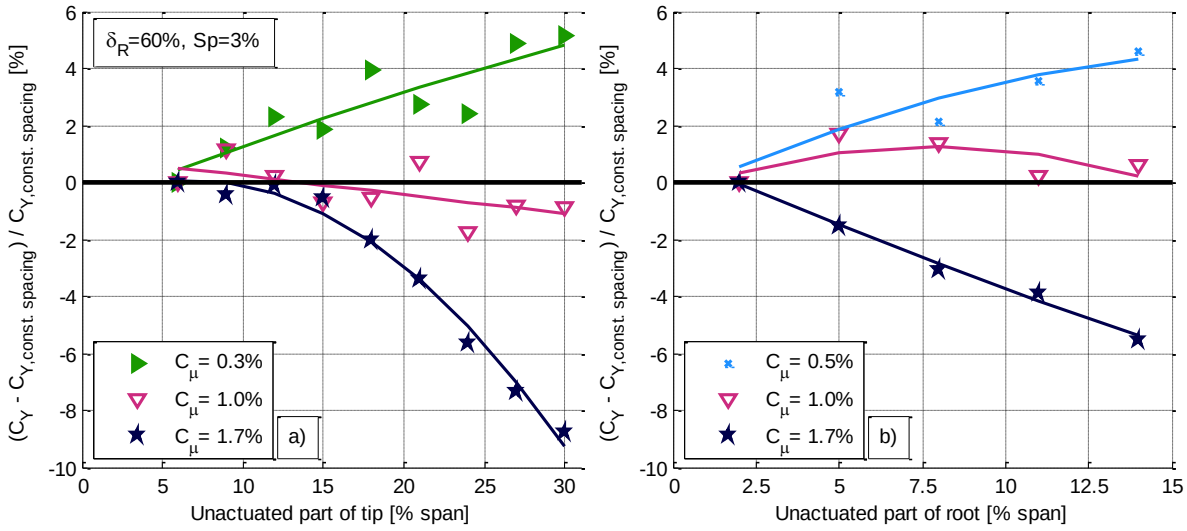

Figure R 9 Effect of removing actuation near the tip (a) or the root (b) at δ_R=60%, β=0° and U_∞=40m/s with Sp=3%, A_{act}=1.

Dividing the span into four equal segments and actuating each segment separately at δ_R=60% generates the side forces shown in Figure R10. The two central segments provide identical results irrespective of C_μ. The lowest segment (1/4span) catches up with the central two when C_μ>0.7%, suggesting that above this threshold level the effect of the root corner and necklace vortices is diminished. The tip segment generates much smaller C_{Yn} than the other three confirming the previous observations. When all four segments were actuated simultaneously the C_{Yn} reached at this spacing was 1.5 at C_μ=1.5%. (Figure R 2), and when the effect of all segments is summed assuming linear superposition the C_{Yn} generated should have been approximately 1.7 at the same C_μ. One may use the same number of actuators that were used in each segment but distribute them equally along the entire span. This eliminates all compressibility effects from the comparison but it requires a gap of 12% span between adjacent actuators. The result indicates that evenly distributed actuators at large distances apart are much more effective than a concentration of actuation in a prescribed region. The figure of merit, FM, provides a very good indication to this effect (Fig. R10 left) since the evenly distributed actuation at the large Sp=12% attains a FM=1.18 while the focused actuation attains at best FM<1.12 using identical total number of actuators. The FM curves peak at 3<C_π<3.5 which should possibly be multiplied by a factor of 4 when compared with actuation using Sp<3% (Fig. R4). These observations imply that a global reorientation of the spanwise flow has an important role in generating the side force.

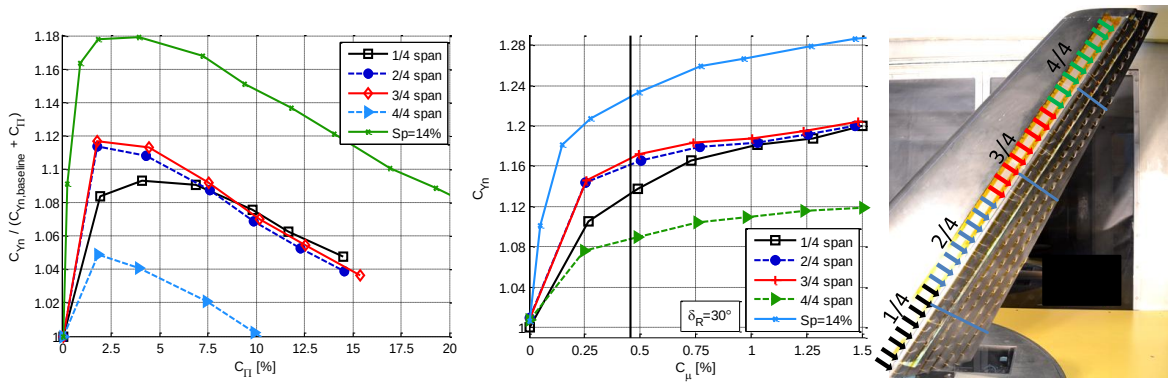

Figure R 10 Comparing the effectiveness of actuating from different spanwise sections with evenly distributed actuation using identical total number of actuators. δ_R=60%, β=0° and u_∞=40m/s with Sp=3%, A_{act}=1 (vertical line in the central figure indicates (U_j=U_c)).

One may ask about the cause for the ineffectiveness of concentrated regional AFC and the best way to explain the physics of the phenomenon is to use one of the two central quarters. Tuft visualization is shown in Figure R 11a where δ_R=60% and the total C_μ=1.5% implying that locally there is a very large concentration of momentum. The flow over the deflected rudder directly downstream of the active sweeping jets is attached. This creates a very low pressure near the rudder hinge that generates a secondary flow toward the actuated region from both above and below its spanwise boundaries. One may clearly observe that the first row of tufts above the actuated region is pointing down (Figure R 11a), while in the absence of actuation these tufts point all up toward the tip (Fig. R10b). The downward entrainment effect is not local because it takes an additional 30% of the span for the tufts to revert to their separated condition. The effect on the root region is opposite since the spanwise jet entrainment pulls flow from below resulting in earlier separation and reduced side force generated by that region.

Chordwise pressure distributions are consistent with the observations obtained by the tufts (Figure R 11c). Measurements taken at approximately 2 actuator spacings below the lowest active sweeping jet actuator (note the green line on Figure R 11a) indicate that the negative pressure peak at the rudder hinge decreased from C_p=-3.2 in the absence of AFC to C_p=-2.5 at C_μ=1.5%. Baseline pressure distribution in the mid section that is above the actuated region suggests that the flow is completely separated over the rudder having approximately C_p=-1 at the trailing edge (Figure R 11c). The application of AFC below this line generates a C_p=-3.6 over the rudder shoulder and it reduces the pressure over the entire tail section at this spanwise location. This low pressure corresponds to the region where the tufts point downward toward the sweeping jets (Figure R 11a). The flow is probably separated over the next fraction of the rudder chord (0.7<x/c<0.8), but the pressure tap line intersects the edge of the sweeping jet at or near the trailing edge of the rudder resulting in an apparent sharp increase in pressure between 0.8<x/c<1.0. The last tuft at the edge of the actuation and the trailing edge is aligned approximately with the free stream direction and this is consistent with the C_p distribution. The flow over the rudder corresponding to the outboard pressure-tap-line is separated but the effect of entrainment is felt even at this spanwise location that is roughly 10 actuator distances above the active jets boundary (Figure R 11c).

Integrating the pressure distribution per unit span provides an integrated side force that is assessed for the entire range of C_μ considered. The effect of the actuation in the second segment has a deleterious effect on the C_{Yn}

generated by the lower section (Figure R 11b). It has a large positive effect on the second array of chordwise pressure taps ("middle section"), due to the jet entrainment that redirects some flow toward the root of the vertical tail. The effect persists toward the tip but it is much weaker there (Figure R 11b). It is interesting to note that these pressure distributions are sensitive to an increase in C_μ as long as the latter is smaller than 0.25%. This number seems deceivingly small, but it represents an overall C_μ that is concentrated over a ¼ of the span. So locally the effect seems to saturate at $C_\mu \approx 1\%$ that bodes well with the integral results achieved for uniform actuation along the span.

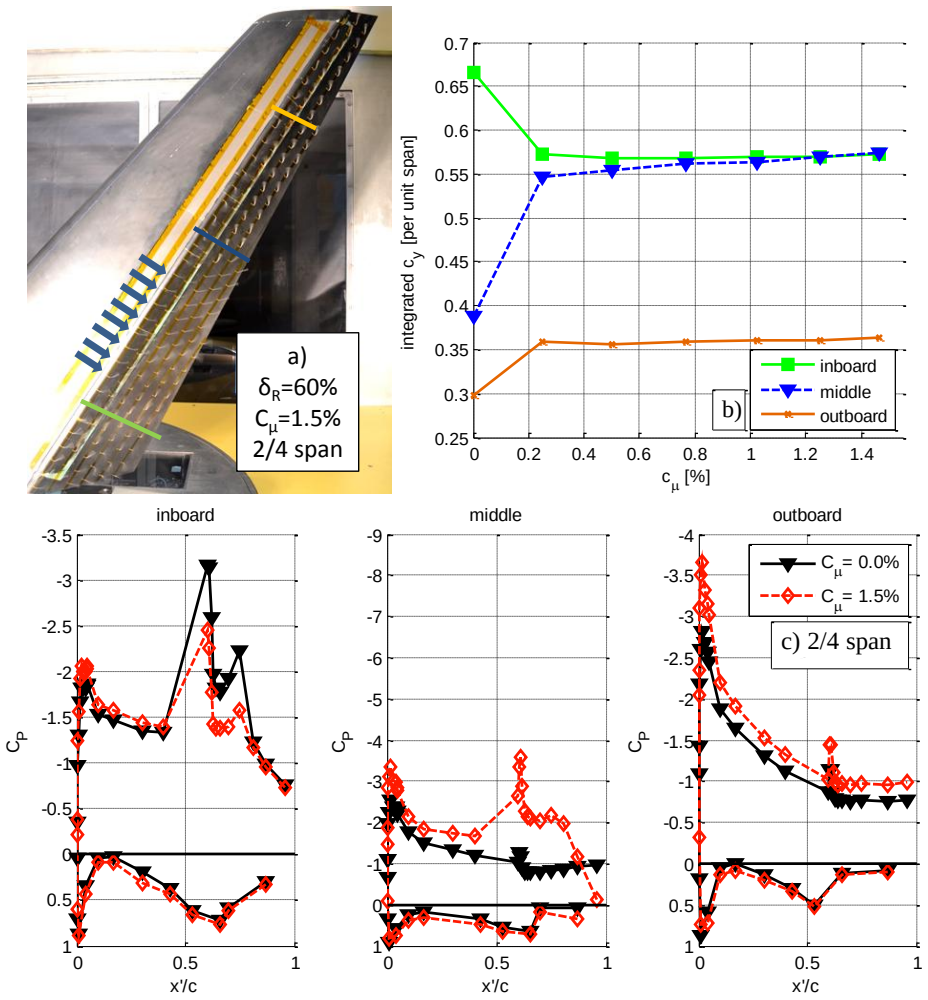

Figure R 11 Concentrating the actuation over the second quarter of the span at δ_R=60%, C_μ =1.5% with A_{act}=1: a) tuft visualization; b) the effect of C_μ on integrated pressure; c) chordwise pressure distributions.

The effect of the sparsely but evenly distributed actuation on the pressure distribution over the rudder is shown in **Figure R 12**. The contours plotted represent the difference between the baseline pressure and the pressure attained by actuators separated by Sp=12%. They were obtained for the rudder only and their physical implications are very clear. Actuation lowered the pressure (red) near the rudder's hinge and it did so almost uniformly across 70% of the span. In all cases considered the pressure is lowered farther downstream around 2/3 of the span. This is not due to the tip vortex that creates an entirely different flow field (not shown) very close to the tip, but it is due to vorticity

that accumulated by the spanwise flow that was being shed off the wing. Positive pressure contours (blue) suggest that the flow is better attached near the trailing edge providing a better pressure recovery (positive) due to the actuation. This is highly non uniform across the span unless the Cμ is high for the rudder deflection used. In the case of lower rudder deflection (δ_R =40%) and Cμ=1.5% the pressure changes distributed along the span are fairly uniform because the magnitude of the spanwise flow was reduced. At the other end of the spectrum very low Cμ=0.3% has a major effect on the pressure distribution near the rudder hinge (Fig. R 13) but the change in the pressure is much more three dimensional farther downstream suggesting that the flow is not fully attached over the entire rudder.

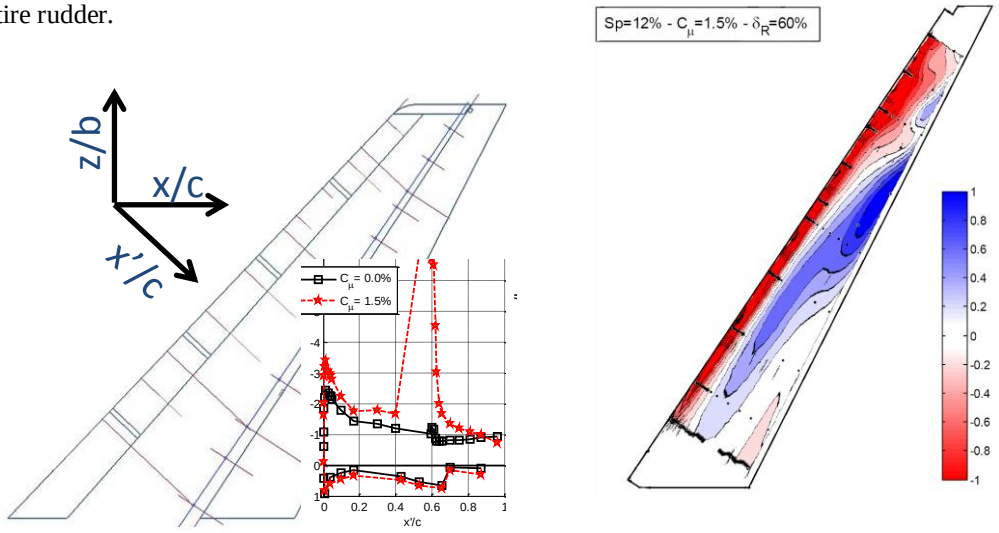

Figure R 12 Pressure contours representing the difference between baseline flow and evenly distributed, sparsely spaced actuation over the rudder. δ_R=60%, C_μ =1.5%, Sp=12%.

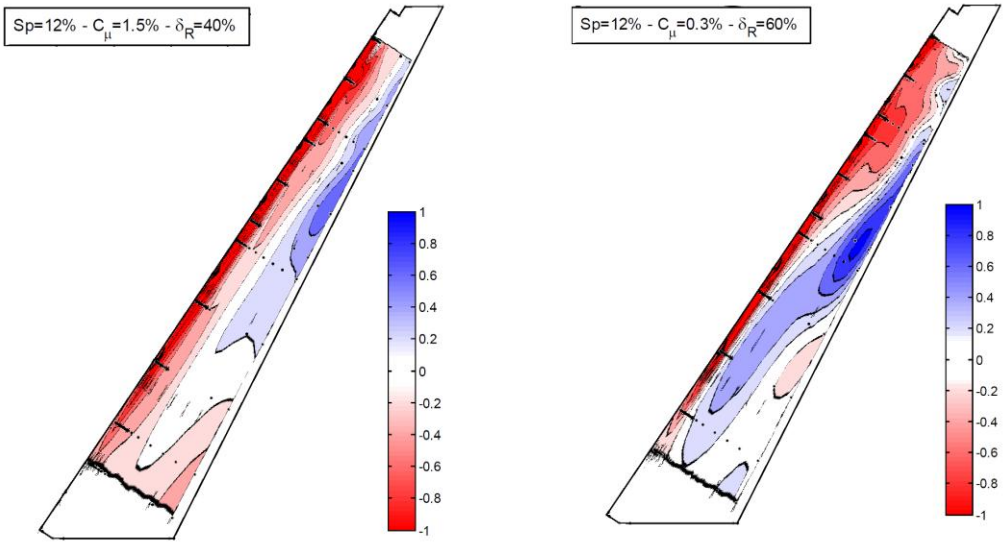

Figure R 13 Pressure contours representing the difference between baseline flow and evenly distributed, but sparsely spaced actuation over the rudder. δ_R=40%, C_μ=1.5%, Sp=12% (left), . δ_R=60%, C_μ=0.3% (right).

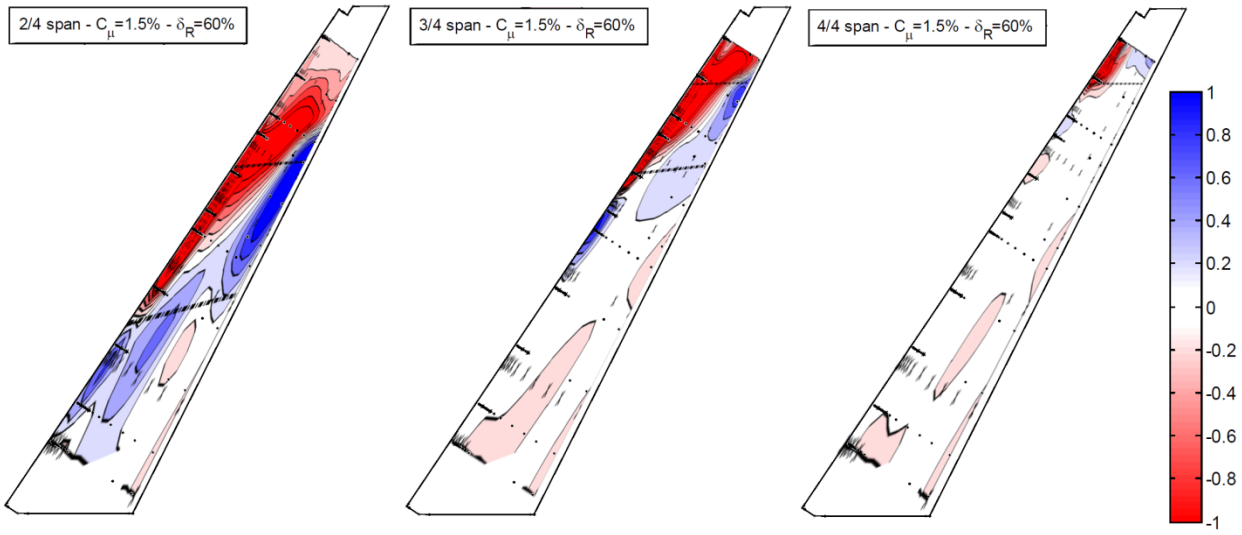

Figure R 14 Pressure contours representing the difference between baseline flow and evenly distributed, sparsely spaced actuation over the rudder. δ_R=60%, C_μ=1.5%, Sp=3%,

Concentrating the same mass flow and momentum onto ¼ of the span at a time attaches the flow over the specific quarter and slightly outboard of it but it has a deleterious effect on the inboard section of the rudder. This effect is clearly seen in Fig. R 14 where actuation from the three top quarters is compared. The pressure below the actuated region increases relative to its baseline because of the strong entrainment of the sweeping jets from above redirects the flow along the span. One concludes that turning the flow inboard, toward the direction of streaming, improves the control authority of the rudder.

INTERIM CONCLUSIONS

The size of the vertical tail on a multi engine airplane is determined by the eventuality of engine loss after takeoff and during climb. It is a large surface that has to provide adequate yaw control during "engine out" emergency. Normal rudder operations, even during cross-wind takeoff or landing are much less demanding. Thus, an increase in rudder efficiency can reduce the drag and weight of a prospective airplane. The vertical tail is a good proving ground for nascent high lift technologies since its maximum lift capabilities are not required for all but a few emergency situations. If the total size of the vertical stabilizer is decreased while the necessary yaw authority for those few critical scenarios can still be maintained by AFC, an added benefit for the entire flight envelope may be achieved.

This report describes experiments carried out on a typical vertical tail of a commercial airplane in order to increase the effectiveness of its rudder. The use of sweeping jets placed on the surface close to the rudder hinge improved the control authority of the rudder by approximately 50% at $C_\mu \approx 1\%$. Notably, almost half of this improvement (i.e. 24%) may be achieved by reducing the spanwise flow over the rudder and that can already be attained at $C_\mu \approx 0.1\%$. Although the task of designing the actuators and their integration into the system is still in progress, there are a few pointers worth mentioning:

1. Most of the benefits that are reaped out at $C_\mu \approx 0.1\%$ are associated with reorientation of the flow and can be achieved by steady jets that are sparsely spaced near the rudder hinge. This observation applies only to highly swept back wings and control surfaces.
2. Reattachment of the flow requires higher C_μ for which the oscillating motion of the sweeping jet actuators is very beneficial.
3. The size of the actuators and the distance measured between adjacent ones determines the effectiveness of the system.
4. Jet velocities should be at least 3 times larger than the free stream for the critical rudder deflection but they should remain subsonic for most effective sweeping motion actuation.
5. There generally is a strong coupling among all variables used to generate large side force on a given vertical tail (e.g. rudder deflection, C_μ, actuator size, aspect ratio, spacing and location).

The proper hierarchy of parameters governing the redirection of the flow and its attachment to the surface becomes more complicated due to the close coupling among geometrical variables (sweep, taper, aspect ratio and rudder hinge location) and AFC (density and size of actuators, their location and orientation relative to the rudder hinge, C_μ, as well as jet velocity relative to the free stream and compressibility effects). In short, there is little chance of collapsing the results onto a single curve as it was reasonably done for 2D flow.

References

[1] Attinello, J.S., "Design and Engineering Features of Flap Blowing Installations" in: Boundary Layer and Flow Control, Its Principles and Application, Lachmann, G.V. (editor), Pergamon Press, New York, 1961.

[2] Stratford, B.S., "Early Thoughts on the Jet Flap". Aeronautical Quarterly, Vol. VII, p. 45, February, 1956.

[3] Poisson-Quinton, Ph., "Recherches Theoriques et Experimentales Sur le Controle de Couche Limites", VII International Congress of Applied Mechanics, London, 1948.

[4] Chen, C., Seele, R., Wygnanski, I., "Separation and Circulation Control on an Elliptical Airfoil by Steady Blowing", AIAA Journal, Vol. 50, No.10, pp. 2235-2247, October 2012

[5] Chen, C., Seele, R., Wygnanski, I., "Flow Control on a Thick Airfoil Using Suction Compared to Blowing", accepted for publication in December 2012, doi: 10.2514/1.J052098

[6] Wygnanski, I. and Newman, BG. "The effect of jet entrainment on lift and moment for a thin aerofoil with blowing", Aero. Quart. XV, pp. 122-150, 1964

[7] Wygnanski, I. "A wind tunnel investigation of a thin aerofoil with a sharp leading edge, and blowing applied at the midchord at two angles relative to the surface", Royal Aeronautical Society, Journal Vol. 70,pp. 665-669, 1966

[8] Woszidlo, R., Nawroth, H., Raghu, S., and Wygnanski, I., "Parametric Study of Sweeping Jet Actuators for Separation Control", AIAA 2010-4247, AIAA 5th Flow Control Conference, 28 June – 1 July, Chicago, Illinois, 2010.

[9] Woszidlo, R. and Wygnanski, I., "Parameters Governing Separation Control with Sweeping Jet Actuators", AIAA 2011-3172, AIAA 29th Applied Aerodynamics Conference, 27-30 June, Honolulu, HI, 2011.

[10] Oster, D. and Wygnanski, I., The forced mixing layer between parallel streams. Journal of Fluid Mechanics, Vol. 123, pp 91-130, 1982, doi:10.1017/S0022112082002973

[11] Seifert, A., Bachar, T., Koss, D., Wygnanski, I., and Shepshelovich, M., "Oscillatory Blowing—A Tool to Delay Boundary-Layer Separation," AIAA Journal 31, 2052-2060, 1993.

[12] Darabi, A., and Wygnanski, I., "Active Management of Naturally Separated Flow Over a Solid Surface. Part 1. The Forced Reattachment Process," Journal of Fluid Mechanics 510, 105-129, 2004.

[13] Darabi, A., and Wygnanski I., "Active Management of Naturally Separated Flow Over a Solid Surface. Part 2. The Separation Process," Journal of Fluid Mechanics 510, 131-144, 2004.

[14] Glezer, A., and Amitay, M.. "Synthetic jets." Annual Review of Fluid Mechanics 34, no. 1 (2002), pp. 503-529.

[15] Sahni, O., Wood, J., Jansen, K. E. and Amitay, M., "3-D Interactions between a Finite-Span Synthetic Jet and a Cross Flow at a Low Reynolds Number and Angle of Attack", Journal of Fluid Mechanics, Vol. 671, pp. 254-287, 2011.

[16] Rathay, N., Boucher, M., Amitay, M. and Whalen, E., "Performance Enhancement of a Vertical Stabilizer using Synthetic Jet Actuators: Non-zero Sideslip", AIAA 2012-2657, 6th AIAA Flow Control Conference 25 - 28 June, New Orleans, LA, 2012

[17] Post, M. L., and Corke, T. C., "Separation Control on High Angle of Attack Airfoil Using Plasma Actuators," AIAA Journal, Vol. 42, No. 11, 2004, pp. 2177–2184.

[18] Greenblatt, D., and Wygnanski, I.. "The control of flow separation by periodic excitation", Progress in Aerospace Sciences 36, no. 7 (2000), pp. 487-545.

[19] Seifert, A., Bachar, T., Wygnanski, I., Kariv, A., Cohen, H., and Yoeli, R., "Application of Active Separation Control to a Small Unmanned Air Vehicle," AIAA Journal of Aircraft 36, 474-477, 1999.

[20] McVeigh, M.A., Nagib, H., Wood, T. and Wygnanski, I., "Full-Scale Flight Tests of Active Flow Control to Reduce Tiltrotor Aircraft Download", Journal of Aircraft, Vol. 48, No. 3 , pp. 786-796, 2011

[21] Seele, R., Graff, E., Gharib, M., Taubert, L., Lin, J. and Wygnanski, I., "Improving Rudder Effectiveness with Sweeping Jet Actuators", AIAA paper 2012-3244, 6th AIAA Flow Control Conference, 25 - 28 June, New Orleans, LA, 2012

[22] Seele, R., Graff, E., Lin, J. and Wygnanski, I., " Performance Enhancement of a Vertical Tail Model with Sweeping Jet Actuators", AIAA Paper 2013-0411, 51st ASM Conference, 7 - 10 January, Grapevine, Texas, 2013

[23] Vatsa, V., Koklu, M and Wygnanski, I., "Numerical Simulation of Fluidic Actuators for Flow Control Applications", AIAA-2012-3239, AIAA 6th Flow Control Conference, 26 – 29 June, New Orleans, LA, 2012.

[24] Phillips, E., Woszidlo, R., and Wygnanski, J., "The Dynamics of Separation Control on a Rapidly Actuated Flap", AIAA 2010-4246, AIAA 5th Flow Control Conference, 28 June-1 July, Chicago, IL, 2010.